Broadband Terahertz Generation via the Interface Inverse Rashba-Edelstein Effect

C. Zhou,[1,*] Y. P. Liu,[2,3,*] Z. Wang,[1] S. J. Ma,[1] M. W. Jia,[1] R. Q. Wu,[1,4] L. Zhou,[1] W. Zhang,[5]
M. K. Liu,[6] Y. Z. Wu,[1,7,†] and J. Qi[2,‡]

[1]*State Key Laboratory of Surface Physics, Department of Physics, Fudan University, Shanghai 200433, China*
[2]*State Key Laboratory of Electronic Thin Films and Integrated Devices,
University of Electronic Science and Technology of China, Chengdu 610054, China*
[3]*Institute of Modern Physics, Fudan University, Shanghai 200433, China*
[4]*Department of Physics and Astronomy, University of California, Irvine, California 92697, USA*
[5]*Department of Physics, Oakland University, Rochester, Michigan 48309, USA*
[6]*Department of Physics, Stony Brook University, Stony Brook, New York 11794, USA*
[7]*Collaborative Innovation Center of Advanced Microstructures, Nanjing 210093, China*

Novel mechanisms for electromagnetic wave emission in the terahertz frequency regime emerging at the nanometer scale have recently attracted intense attention for the purpose of searching next-generation broadband THz emitters. Here, we report broadband THz emission, utilizing the interface inverse Rashba-Edelstein effect. By engineering the symmetry of the Ag/Bi Rashba interface, we demonstrate a controllable THz radiation (∼0.1–5 THz) waveform emitted from metallic Fe/Ag/Bi heterostructures following photoexcitation. We further reveal that this type of THz radiation can be selectively superimposed on the emission discovered recently due to the inverse spin Hall effect, yielding a unique film thickness dependent emission pattern. Our results thus offer new opportunities for versatile broadband THz radiation using the interface quantum effects.

Terahertz radiation from 0.1–30 THz accesses a diverse group of low-energy elementary excitations in solid-state systems [1], holding great promises for imaging, sensing, and security applications [2]. One major challenge in the next generation THz technology is to search novel mechanism(s) providing efficient and broadband THz radiation with a gapless spectrum [3–5]. To date, most broadband THz emission devices [2–5] are based on the femtosecond laser excitations, taking advantage exclusively of the nonlinear or dynamic properties of the electrons. Recently, the emerging ultrafast spintronics [6–13], however, offers an alternative route to the THz emission with the spin degree of freedom, by converting spin current bursts into THz pulses. In this way, one can effectively generate, control, and detect the spin currents, as well as utilize such spin-to-charge conversion [6–13] within the subpicosecond timescale to yield efficient ultrabroadband THz emission. Such ultrafast spin-to-charge conversion process in all previous works is mostly based on the inverse spin Hall effect (ISHE) [14,15], which happens inside the bulk of a metallic system with a strong spin-orbit coupling (SOC).

In contrast, the inverse Rashba-Edelstein effect (IREE) occurring at the interfaces with broken inversion symmetry can also provide efficient spin-to-charge conversion [16–19]. In the IREE, the generated charge current in two-dimensional electron gas can be described by [19]

$$\mathbf{j_c} \propto \lambda_{\text{IREE}} \mathbf{j_s} \times \hat{\mathbf{z}}, \tag{1}$$

where λ_{IREE} is the IREE coefficient which is proportional to the Rashba parameter α_R, $\hat{\mathbf{z}}$ is the direction of the potential gradient (interfacial electric field) perpendicular to the interface, and $\mathbf{j_s}$ is the spin current. Although the IREE has been intensively studied under equilibrium or quasiequilibrium conditions in magnetoresistance measurements [17], nonlocal spin valves [18], and ferromagnetic resonance experiments [19], it is still elusive whether the IREE can work in femtosecond timescale, and play a vital role in the THz emission.

In this work, we report the observation of THz radiation via the interface IREE in the metallic Fe/Ag/Bi heterostructures, which strongly suggests the effect of the interface IREE on the spin-to-charge conversion in femtosecond timescale. This observation brings us to a novel mechanism of emitting broadband THz wave from interface states, in contrast to the others based on the bulk properties dominating mainstream THz sources. In addition, the THz emission spectroscopy is also demonstrated to be an indirect way to reveal the evolution of the SOC-related electronic properties at the Ag/Bi interfaces.

Figure 1(a) shows the scheme for an IREE-based THz emitter, which is a metallic heterostructure consisting of ferromagnetic (FM) and two nonferromagnetic (NM$_1$ and NM$_2$) thin films. The Rashba SOC exists between NM$_1$ and
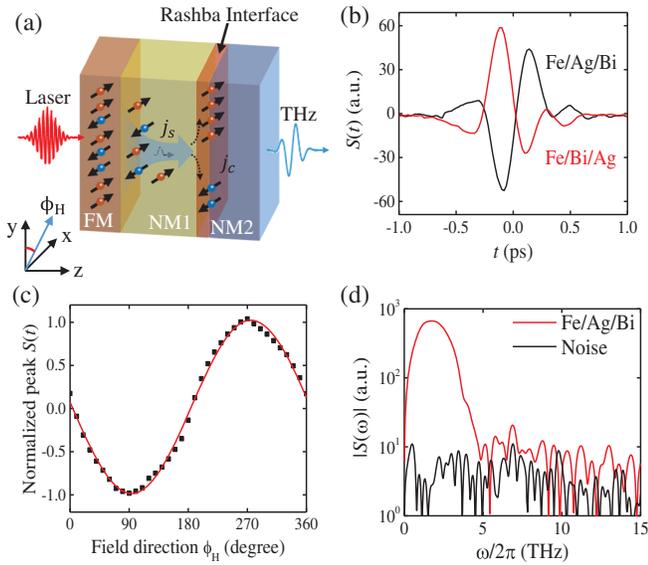
FIG. 1. (a) Schematic of THz emission via IREE upon excitation of ultrafast laser pulses. (b) Typical time-domain THz signals in Fe(2)/Ag(2)/Bi(3) and Fe(2)/Bi(3)/Ag(2) films. (c) Normalized peak $S(t)$ versus direction of the external magnetic field together with a sinusoidal curve, measured on a Fe(2)/Ag(2)/Bi(3) film. THz detection is optimized along the y axis. (d) The frequency-domain THz signal in Fe/Ag/Bi corresponding to the time-domain signal in (b). Background noise is also shown in (d). The number inside each pair of brackets indicates the corresponding film thickness in nanometer.

NM_2. The FM film is magnetized by an in-plane magnetic field. A femtosecond laser pulse excites the heterostructure and leads to the generation of nonequilibrium spin-polarized electrons in the FM film [20], which subsequently super-diffuse across the neighboring NM_1, known as the spin current, and arrive at the NM_1/NM_2 Rashba interface. Because of the IREE, this longitudinal spin current $\mathbf{j}_s$ at the interface converts into a transient transverse charge current $\mathbf{j_c}$, which thereby acting as a source of THz radiation. Here, we select Ag and Bi as the two NM films, because the Ag/Bi interface is proved to have strong Rashba SOC between Bi(111) and Ag [19,21,22]. We first epitaxied a 2 nm Fe film on MgO(001) substrate, then grew either Ag/Bi or Bi/Ag bilayer on top of the Fe film. The *in situ* reflection high-energy electron diffraction indicates that the Ag film on top of Fe film is single crystalline, but the Bi film is polycrystalline. The THz emission spectroscopy experiments were performed at room temperature. More experimental details about the samples and our THz emission spectroscopy setup are shown in the Supplemental Material [23].

Figure 1(b) illustrates the typical time-domain THz signals detected in two trilayer samples Fe(2)/Ag(2)/Bi(3) and Fe(2)/Bi(3)/Ag(2). The number inside each pair of brackets indicates the corresponding film thickness in nanometer. Obviously, the THz signals in these two samples are almost the same in shape and strength. A crucial observation is that the signals are completely out of phase once the stacking

order of Bi/Ag is reversed. The THz signals from Fe/Bi and Fe/Ag bilayers are much smaller than those from Fe/Ag/Bi and Fe/Bi/Ag trilayer samples. Such observation is a direct evidence of THz radiation arising from the IREE-based spin-to-charge conversion. This is because when the stacking order of Bi and Ag is changed, the direction of the interfacial electric field is reversed (from $\hat{\mathbf{z}}$ to $-\hat{\mathbf{z}}$). According to Eq. (1), this will lead to a sign reversal of the charge current, and hence the THz emission, as demonstrated in Fig. 1(b). We note that this result is in sharp contrast to the signal reversal via ISHE [6,9], where the direction of the spin current has to be reversed. In the current situation, the direction of the spin current is same since the relative position between the FM layer and the NM layers is not changed. It should be noted that, if rotating the in-plane magnetization, the angular-dependent THz signal shows a clear sine-shape dependence [see Fig. 1(c)], which is expected by the IREE effect [see Eq. (1)].

Figure 1(d) shows that a typical broad bandwidth from ~0.1 to 5 THz, peaking at around 2 THz, can be obtained in these samples. The maximum electric field in these two samples is evaluated to be ~1.3 V/cm, which is only about 6 times smaller than that in a ZnTe (110) crystal with a thickness of 1 mm measured under the same experimental conditions [23]. Such result is really remarkable if the THz signals from Fe/Ag/Bi are solely attributed to the IREE, because generally the effective thickness of the active Rashba interface is a monolayer (ML), which is almost 7 orders of magnitude smaller than that of the conventional nonlinear crystals. Strength of the peak electric field also suggests that IREE, in terms of the THz emission, is far superior to the other interface inverse spin-orbit torque effect [7] (Ref. [7] used a laser fluence of 1 mJ/cm², which is larger than ours by 2 orders of magnitude.), and can be comparable with the bulk ISHE [6,8–13]. Therefore, IREE may offer a novel mechanism in generating the efficient broadband THz wave.

In order to further clarify and optimize the IREE-based THz emission, we have carried out control experiments on three samples: Fe(2)/Bi(d_{Bi}), Fe(2)/Bi(d_{Bi})/Ag(2), and Fe(2)/Ag(2)/Bi(d_{Bi}), where the Bi layer is wedge shaped with its thickness d_{Bi} increasing continuously from 0 to 4 nm. Figures 2(a)–2(c) illustrate the typical THz signals measured in these three samples with different thicknesses. In general, the Fe/Ag/Bi and Fe/Bi/Ag trilayers yield much stronger THz signals than Fe/Bi and Fe/Ag (d_{Bi} or $d_{Ag} = 0$ nm, and also see the Supplemental Material [23]), which produce a comparable THz emission with a single layer of Fe ($d_{Bi} = 0$ nm). These results can exclude the following effects dominantly contributing to the observed signals in trilayer samples: (i) demagnetization in Fe film [37], (ii) ISHE in bulk Bi or Ag, (iii) and potential signals from other interface states, e.g., Fe/Bi. Thus, our results are well consistent with recent work by M. Jungfleisch [38], where the enhancement of THz emission in CoFeB/Ag/Bi was understood by the IREE at the Rashba Ag/Bi interface.
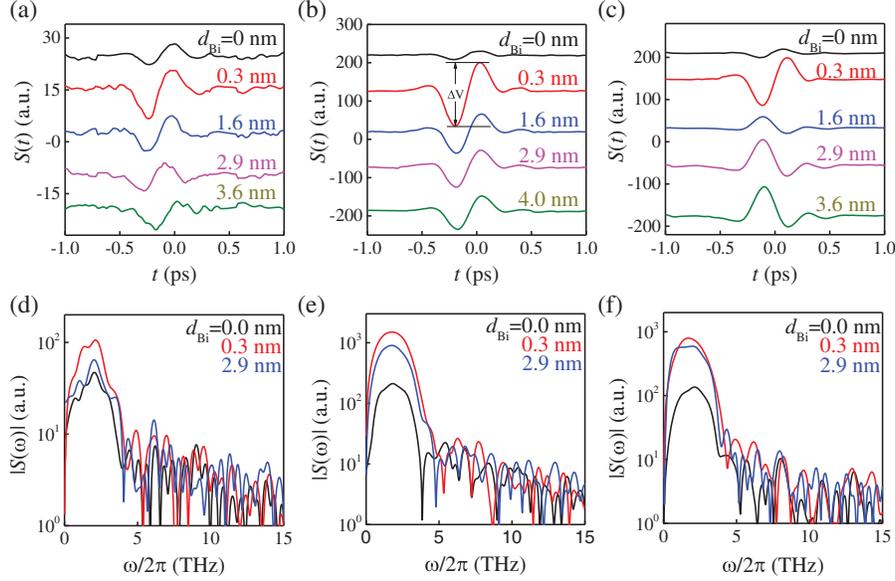
FIG. 2. Typical time-domain THz signals at different Bi thickness for (a) Fe(2)/Bi(wedge), (b) Fe(2)/Ag(2)/Bi(wedge), and (c) Fe(2)/Bi(wedge)/Ag(2). The corresponding frequency-domain signals are shown in (d)–(f), respectively. The number inside each pair of brackets indicates the corresponding film thickness in nanometer.

However, the THz signals obtained in Fe/Ag/Bi and Fe/Bi/Ag are not always out of phase, and even exhibit very different magnitudes in the low thickness regime. To understand such unusual behavior, we performed detailed Bi-thickness dependent analysis of the trilayer samples, whose structures are simply depicted in Figs. 3(a)–3(b). We define the amplitude ΔV as the peak-to-valley difference between the largest and smallest values in signal $S(t)$. Figure 3(c) shows the linear dependence between the amplitude of the THz wave and the pump laser fluence in our experimental condition, which indicates that the photon-induced spin current density linearly depends on the optical intensity in the Fe layer. Under the current situation where the bandwidth, from ~0.1 to 5 THz, almost does not change with Bi thickness for each trilayer sample, the thickness dependence of THz signal can be largely manifested by ΔV as a function of d_{Bi}. $\Delta V(d_{Bi})$ obtained in Fe/Ag/Bi and Fe/Bi/Ag are shown in Fig. 3(d). Dependence of ΔV on d_{Bi} here is very different from that of the Co/Pt bilayers, where ISHE is the main mechanism for THz emission [23].

In an ideal IREE case, only the ultrafast spin current ($\mathbf{j_s}$) arrived at Rashba interface plays the role of THz emission [yellow regions in Figs. 3(a)–3(b)]. Therefore, in Fe/Ag/Bi with constant d_{Ag}, for a given spin current density, one should expect that the amplitude of the THz wave is independent on the Bi thickness for a well-established Rashba interface. However, Fig. 3(d) shows that the THz radiation in Fe/Ag/Bi decreases gradually with the Bi thickness for $d_{Bi} > 0.5$ nm. This result can arise from the influence of the NM layer thickness on the optical intensity in the Fe layer, which determines the ultrafast spin current intensity. Such influence was revealed by the

calculations using the transfer matrix method [23], which deals with the multiple optical reflection effect [8]. Because the hot-electron spin density in FM metals close to the FM/NM interface provides the dominant source of ultrafast spin current [6,20] [shaded regions in Figs. 3(a)–3(b)], we can only focus on the optical intensity (or optical absorption) in the Fe part near Fe/Ag or Fe/Bi interface. Figure 3(e) shows the normalized optical intensity I_O near the FM/NM interface in Fe/Ag/Bi and Fe/Bi/Ag as a function of d_{Bi}, which almost decreases exponentially with d_{Bi}. This finding demonstrates that as the NM layer thickness ($d_{NM} = d_{Bi} + d_{Ag}$) increases, the laser intensity at the FM/NM interface drops, and hence reduces the ultrafast spin current density and its associated THz radiation. Such a dropping effect can be numerically eliminated by normalizing the THz signals using the calculated optical intensity above, as shown in Fig. 3(f). We can see that the signal in Fe/Ag/Bi is almost independent of the Bi thickness for $d_{Bi} > 0.5$ nm, which confirms the above expectation for a perfect IREE-based THz emission.

However, the normalized THz signal for Fe/Bi/Ag in Fig. 3(f) still decreases with increasing d_{Bi}, although the Rashba interface should be already well established for $d_{Bi} > 3$ nm. Such observation might be attributed to the decay of the spin current density traveling through the Bi layer. This decay leads to the spin current density $j_s(d_{Bi})$ at Ag/Bi interface determined by $j_s(d_{Bi}) \propto \exp(-d_{Bi}/\lambda_s^{Bi})$, where λ_s^{Bi} is the spin diffusion length. It should be noted that the possible backflow [39,40] of the spin current from the interface between Ag and MgO capping layer may also influence the THz emission from the Ag/Bi interface.
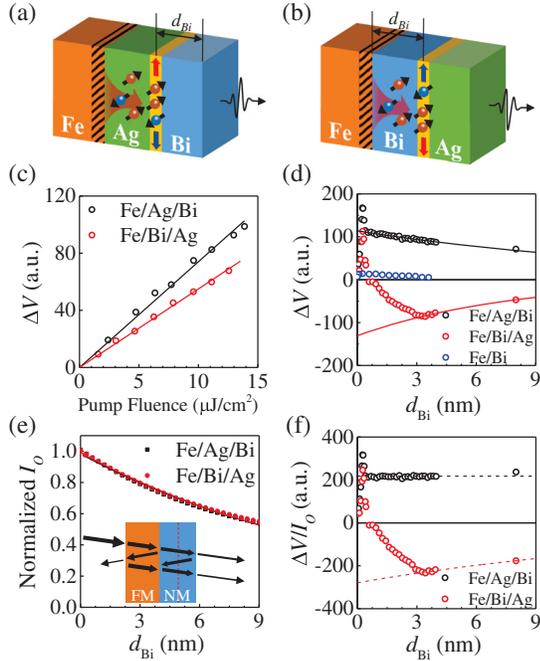
FIG. 3. Schematics of key parameters determining the thickness dependence of THz signals in (a) Fe/Ag/Bi and (b) Fe/Bi/Ag. The yellow regions indicate the Rashba interfaces. (c) Peak-to-peak amplitude ΔV as a function of laser pump fluence in Fe(2)/Ag(2)/Bi(2) and Fe(2)/Bi(2)/Ag(2). Solid lines are linear fittings. (d) Peak-to-peak amplitude ΔV as a function of Bi thickness in Fe/Ag/Bi, Fe/Bi, and Fe/Bi/Ag films. The solid lines are exponential fitting. (e) Normalized optical intensity I_O in the Fe layer near the FM/NM interface as a function of Bi thickness calculated by the transfer matrix method. The inset is the schematic of multiple reflections. (f) The THz signal normalized by the calculated optical intensity I_O in the Fe/Ag/Bi and Fe/Bi/Ag films. The black and red dashed lines are constant and exponential decay fitting, respectively.

However, since Fe/Bi/Ag has the constant Ag thickness with all interfaces well established for $d_{\mathrm{Bi}} > 3$ nm, the backflow spin current at the Bi/Ag interface should be also proportional to $j_s(d_{\mathrm{Bi}})$, i.e., $\propto \exp(-d_{\mathrm{Bi}}/\lambda_s^{\mathrm{Bi}})$. In fact, the constant $\Delta V/I_O$ ($d_{\mathrm{Bi}} > 0.4$ nm) for Fe/Ag/Bi may indicate the negligible backflow effect. Therefore, $\Delta V/I_O$ (>3 nm) for Fe/Bi/Ag can be fitted using the above exponential decay [see Fig. 3(f)], where the fitted λ_s^{Bi} has a value of $\sim$17 nm. We note that absorption of the THz wave inside our samples can be neglected because its absorption length has a scale of $\sim$100 nm [23].

In Fig. 3(d), a sharp increase and decrease of ΔV across $\sim$0.3 nm is observed in both trilayer samples. As stated, Eq. (1) is valid only if a perfect Rashba interface exists between Ag and Bi at all d_{Bi}. In reality, such conditions can be hardly satisfied. Particularly, a prominent phenomenon discovered previously shows that upon deposition of the first few monolayers Bi, there could appear the AgBi surface alloying with strong SOC [21,22,41]. This is
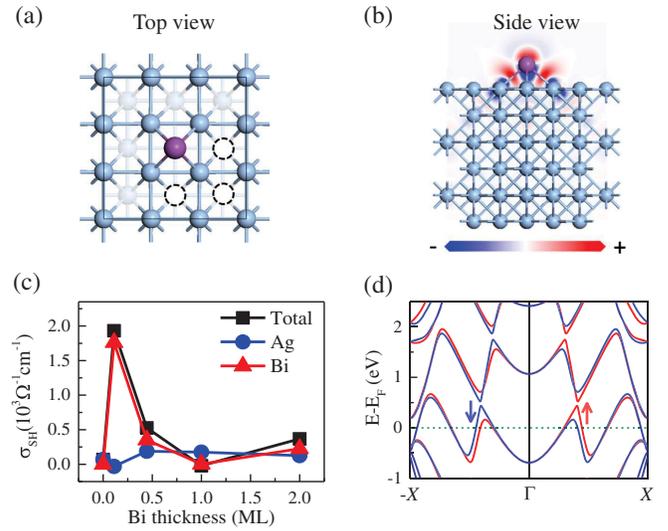

FIG. 4. (a) and (b) Schematic of the supercell for calculations of Bi atoms deposited on Ag(001) from the top view and side view, respectively. The color inside (b) represents the charge redistribution between the adsorbed Bi atom and Ag(001) surface. (c) Spin Hall conductivity as a function of Bi thickness associated with Ag, Bi, and total (Ag + Bi), respectively. (d) The spin-resolved electronic band structure of Bi(1 ML)/Ag(001) along the Γ-X direction, with the red (blue) color representing the spin-resolved band with the spin polarization along the $+y$ ($-y$) direction.

similar to the diluted CuBi alloy system, where a small amount of Bi impurities ($<$0.5%) in Cu could induce a large spin Hall effect [42]. Therefore, we also expect the existence of non-negligible SHE when d_{Bi} is very small. In order to further understand the spin Hall conductivity (SHC) of Bi/Ag bilayers with different Bi thickness, we conducted the first-principles density functional theory calculations, using the projector augmented wave method [43,44] as implemented in the Vienna *ab initio* simulation package (VASP) [45,46]. More calculation details are shown in the Supplemental Material [23]. The Ag(001) substrate was simulated by a six-layer slab with a $3 \times 3 \times 1$ supercell. We placed different numbers of Bi atoms on the Ag surface [see Figs. 4(a)–4(b)], which can be regarded as different Bi coverage in the experiments. Typically, we performed the calculation with the 1/9, 4/9, 1, and 2 ML Bi coverage. Figure 4(c) demonstrates that the calculated intrinsic SHC reaches its maximum (1931 Ω^{-1} cm^{-1}) at 1/9 ML Bi, and is greatly suppressed by further Bi coverage. This result is consistent with the observation that the THz radiation experiences a sharp increase and decrease across a submonolayer Bi thickness, i.e., $\sim$0.3 nm. By selectively switching off the spin-orbit interactions of Bi and Ag atoms, we demonstrate that the SHC is mainly contributed by Bi atoms [Fig. 4(c)]. Although during the calculation we only considered the case where the Bi atoms grow on top of the Ag film, the

remarkable SHC can also be expected to exist in the system with Ag atoms grown on top of Bi.

The Rashba effect in the Bi/Ag(001) system can also be revealed by the theoretical calculation. Figure 4(d) shows that the calculated spin-projected band structures along $-X \rightarrow \Gamma \rightarrow X$ of 1 ML Bi on Ag(001) surface. Because of the hybridization between the Ag s electron and the Bi p electron, there is a clear spin-orbit splitting in the bands across a large energy range. This band splitting only locates inside the Bi layer and the first Ag layer, confirming the existence of the Rashba effect due to the inversion-symmetry broken at the Bi/Ag interface with thickness-scale of 1 ML. Clearly, the THz radiation via IREE will involve a 180° phase change by altering the Bi/Ag interface symmetry via switching the Bi and Ag stacking order.

Therefore, for $0 < d_{Bi} < 0.5$ nm we have observed a superposition of the THz signals via ISHE and IREE in both samples. Such superposition can be manipulated by controlling the symmetry of the Ag/Bi interface. In specific, the superposition is constructive and destructive for Fe/Ag/Bi and Fe/Bi/Ag, respectively. This finding well explains the sign change of ΔV in Fe/Bi/Ag. However, in this sample, quantitatively describing the gradual thickness-dependent signal for $0.5 < d_{Bi} < 3$ nm is still quite challenging. In our experiments, the Ag/Fe bilayer is grown epitaxially on MgO(001) substrate. In contrast, due to the large lattice mismatch between Bi and Fe, Bi grown on Fe(001) film is mostly polycrystalline. This leads to the subsequent nonepitaxial growth of Ag film. Then, the Bi/Ag Rashba interface for Fe/Bi/Ag is expected to slowly establish as the number of the deposited Bi atoms increases, in contrast to the case of Fe/Ag/Bi. Thus, the corresponding critical Bi thicknesses to fully develop the Rashba interface are ~3 and ~0.5 nm for Fe/Bi/Ag and Fe/Ag/Bi, respectively. Therefore, accurate modeling of the Rashba interface requires further investigations using different experimental and theoretical approaches. Nevertheless, our findings provide indirect evidence of the gradual evolution of electronic properties associated with SOC at Ag/Bi interfaces.

In fact, λ_{IREE} can be hardly obtained experimentally because it is impossible to directly determine the ultrafast spin current from the THz signals [6]. Here, we present a rough estimation of the IREE coefficient λ_{IREE} using the THz signals in Fe/Ag/Bi and Fe/Bi. Previous spin pumping work [19,47] reported that the IREE-based signals from trilayers with Ag/Bi interface are larger by a factor between 5 and 12.5 than the ISHE-based signals from bilayers with Bi film. λ_{IREE} was given to be 0.11 and 0.3 nm, respectively. Figure 3(d) shows that the IREE-based signal in Fe/Ag/Bi is 9 times larger than the ISHE-based one in Fe/Bi. If we assume the spin Hall angle and the spin diffusion length in Bi layer are same as those in Refs. [19,48], λ_{IREE} in Fe/Ag/Bi is approximated to be between 0.08 and 0.54 nm. Moreover, Fig. 3(d) also suggests that the THz signal due to the ISHE in

thin BiAg alloy is about 8 times of that in Fe/Bi. Because the spin Hall angle θ_{SH} of the Bi layer varies from 0.008 to 0.02 [48–50], θ_{SH} of the AgBi interface alloy can also be estimated to be ~0.064–0.16.

In summary, our results provide strong indications that the IREE can induce the ultrafast spin-to-charge conversion at subnanometer interfaces, which can be an effective way for generating broadband THz emission at room temperature. The bandwidth of such THz wave dominantly covers ~0.1 to 5 THz. Its phase can be changed by controlling the inversion symmetry at the Ag/Bi and Bi/Ag interfaces. Therefore, our work provides an encouraging example of how the THz emitters via interface Rashba effect can achieve performances close to their bulk counterparts. Our results also demonstrate that THz radiation arising from both IREE and ISHE can superimpose with each other. Therefore, the emission efficiency can be further improved by utilizing both effects in the same device. Finally, we demonstrate the THz emission spectroscopy can be a useful way to reveal the evolution of the electronic properties associated with the SOC at interfaces or surfaces, where many peculiar quantum effects often emerge.

---

*C.Z. and Y.P.L. contributed equally to this work.
†wuyizheng@fudan.edu.cn
‡jbqi@uestc.edu.cn

 [1] S. L. Dexheimer, *Terahertz Spectroscopy: Principles and Applications* (CRC Press, Boca Raton, 2007).
 [2] M. Tonouchi, Nat. Photonics **1**, 97 (2007).
 [3] S. S. Dhillon, M. S. Vitiello, E. H. Linfield, A. G. Davies, M. C. Hoffmann, J. Booske, C. Paoloni, M. Gensch, P. Weightman, G. P. Williams *et al.*, J. Phys. D **50**, 043001 (2017).
 [4] B. Ferguson and X. Zhang, Nat. Mater. **1**, 26 (2002).
 [5] R. A. Lewis, J. Phys. D **47**, 374001 (2014).
 [6] T. Kampfrath, M. Battiato, P. Maldonado, G. Eilers, J. Nötzold, S. Mährlein, V. Zbarsky, F. Freimuth, Y. Mokrousov, S. Blügel, M. Wolf, I. Radu, P. M. Oppeneer, and M. Münzenberg, Nat. Nanotechnol. **8**, 256 (2013).
 [7] T. J. Huisman, R. V. Mikhaylovskiy, J. D. Costa, F. Freimuth, E. Paz, J. Ventura, P. P. Freitas, S. Blügel, Y. Mokrousov, TH. Rasing, and A. V. Kimel, Nat. Nanotechnol. **11**, 455 (2016).

 [8] T. Seifert *et al.*, Nat. Photonics **10**, 483 (2016).
 [9] D. Yang, J. Liang, C. Zhou, L. Sun, R. Zheng, S. Luo, Y. Wu, and J. Qi, Adv. Opt. Mater. **4**, 1944 (2016).
[10] Y. Wu, M. Elyasi, X. Qiu, M. Chen, Y. Liu, L. Ke, and H. Yang, Adv. Mater. **29**, 1603031 (2017).
[11] J. Walowski and M. Münzenberg, J. Appl. Phys. **120**, 140901 (2016).
[12] T. J. Huisman and T. Rasing, J. Phys. Soc. Jpn. **86**, 011009 (2017).
[13] G. Torosyan, S. Keller, L. Scheuer, R. Beigang, and E. T. Papaioannou, Sci. Rep. **8**, 1311 (2018).
[14] J. Sinova, S. O. Valenzuela, J. Wunderlich, C. H. Back, and T. Jungwirth, Rev. Mod. Phys. **87**, 1213 (2015).
[15] A. Hoffmann, IEEE Trans. Magn. **49**, 5172 (2013).
[16] V. M. Edelstein, Solid State Commun. **73**, 233 (1990).
[17] H. Nakayama, Y. Kanno, H. An, T. Tashiro, S. Haku, A. Nomura, and K. Ando, Phys. Rev. Lett. **117**, 116602 (2016).
[18] M. Isasa, M. C. Martínez-Velarte, E. Villamor, C. Magén, L. Morellón, J. M. De Teresa, M. R. Ibarra, G. Vignale, E. V. Chulkov, E. E. Krasovskii, L. E. Hueso, and F. Casanova, Phys. Rev. B **93**, 014420 (2016).
[19] J. C. Rojas Sanchez, L. Vila, G. Desfonds, S. Gambarelli, J. P. Attané, J. M. De Terasa, C. Magén, and A. Fert, Nat. Commun. **4**, 2944 (2013).
[20] M. Battiato, K. Carva, and P. M. Oppeneer, Phys. Rev. Lett. **105**, 027203 (2010).
[21] G. Bian, X. Wang, T. Miller, and T. C. Chiang, Phys. Rev. B **88**, 085427 (2013).
[22] C. R. Ast, J. Henk, A. Ernst, L. Moreschini, M. C. Falub, D. Pacilé, P. Bruno, K. Kern, and M. Grioni, Phys. Rev. Lett. **98**, 186807 (2007).
[23] See Supplemental Material at http://link.aps.org/supplemental/10.1103/PhysRevLett.121.086801 for details on sample growth, THz emission spectroscopy, sample quality, calculation methods, and experimental data, which includes Refs. [24–36].
[24] P. Yeh, *Optical Wave in Layered Media* (Wiley, New York, 1988).
[25] K. Busch, C. T. Chan, and C. M. Soukoulis, *Photonic Band Gap Materials*, edited by C. M. Soukoulis (Kluwer, Dordrecht, 1996).
[26] E. D. Palik, *Handbook of Optical Constants of Solids.* (Academic Press, San Diego, 1985).
[27] R. Iguchi and E. Saitoh, J. Phys. Soc. Jpn. **86**, 011003 (2017).
[28] K. Ando, S. Takahashi, J. Ieda, Y. Kajiwara, H. Nakayama, T. yoshino, K. Harii, Y. Fujikawa, M. Matsuno, S. Maekawa, and E. Saitoh, J. Appl. Phys. **109**, 103913 (2011).
[29] J. Bass and W. P. Pratt, Jr., J. Phys. Condens. Matter **19**, 183201 (2007).
[30] J. C. Rojas-Sánchez, N. Reyren, P. Laczkowski, W. Savero, J.-P. Attané, C. Deranlot, M. Jamet, J.-M. George, L. Vila, and H. Jaffrès, Phys. Rev. Lett. **112**, 106602 (2014).
[31] H. L. Wang, C. H. Du, Y. Pu, R. Adur, P. C. Hammel, and F. Y. Yang, Phys. Rev. Lett. **112**, 197201 (2014).
[32] Z. Feng, J. Hu, L. Sun, B. You, D. Wu, J. Du, W. Zhang, A. Hu, Y. Yang, D. M. Tang, B. S. Zhang, and H. F. Ding Phys. Rev. B **85**, 214423 (2012).
[33] O. Mosendz, J. E. Pearson, F. Y. Fradin, G. E. W. Bauer, S. D. Bader, and A. Hoffmann, Phys. Rev. Lett. **104**, 046601 (2010).
[34] H. Hirori, A. Doi, F. Blanchard, and K. Tanaka, Appl. Phys. Lett. **98**, 091106 (2011).
[35] J. P. Perdew, K. Burke, and M. Ernzerhof, Phys. Rev. Lett. **77**, 3865 (1996).
[36] G. Y. Guo, S. Murakami, T. W. Chen, and N. Nagaosa, Phys. Rev. Lett. **100**, 096401 (2008).
[37] D. J. Hilton, R. D. Averitt, C. A. Meserole, G. L. Fisher, D. J. Funk, J. D. Thompson, and A. J. Taylor, Opt. Lett. **29**, 1805 (2004).
[38] M. B. Jungfleisch, Q. Zhang, W. Zhang, J. E. Pearson, R. D. Schaller, H. Wen, and A. Hoffmann, Phys. Rev. Lett. **120**, 207207 (2018).
[39] H. J. Jiao and G. E. W. Bauer, Phys. Rev. Lett. **110**, 217602 (2013).
[40] X. Qiu, W. Legrand, P. He, Y. Wu, J. Yu, R. Ramaswamy, A. Manchon, and H. Yang, Phys. Rev. Lett. **117**, 217206 (2016).
[41] I. M. McLeod, V. R. Dhanak, A. Matilainen, M. Lahti, K. Pussi, and K. H. L. Zhang, Surf. Sci. **604**, 1395 (2010).
[42] Y. Niimi, Y. Kawanishi, D. H. Wei, C. Deranlot, H. X. Yang, M. Chshiev, T. Valet, A. Fert, and Y. Otani, Phys. Rev. Lett. **109**, 156602 (2012).
[43] P. E. Blochl, Phys. Rev. B **50**, 17953 (1994).
[44] G. Kresse and D. Joubert, Phys. Rev. B **59**, 1758 (1999).
[45] G. Kresse and J. Furthmuller, Phys. Rev. B **54**, 11169 (1996).
[46] G. Kresse and J. Furthmuller, Comput. Mater. Sci. **6**, 15 (1996).
[47] W. Zhang, M. B. Jungfleisch, W. Jiang, J. E. Pearson, and A. Hoffmann J. Appl. Phys. **117**, 17C727 (2015).
[48] H. Emoto, Y. Ando, Y. Fuseya, T. Shinjo, and M. Shiraishi, J. Appl. Phys. **115**, 17C507 (2014).
[49] J. Fan and J. Eom, Appl. Phys. Lett. **92**, 142101 (2008).
[50] S. Sangiao, J. M. De Teresa, L. Morellon, I. Lucas, M. C. Martinez-Velarte, and M. Viret, Appl. Phys. Lett. **106**, 172403 (2015).